Supplement of Atmos. Chem. Phys., 21, 15081–15101, 2021
https://doi.org/10.5194/acp-21-15081-2021-supplement

Supplement of

Time-dependent source apportionment of submicron organic aerosol for a rural site in an alpine valley using a rolling positive matrix factorisation (PMF) window

Gang Chen et al.

Correspondence to: André S. H. Prévôt (andre.prevot@psi.ch)

Table of Contents

S1 Determination of Collection Efficiency (CE)

The CE value typically depends on the particulate water content (Matthew et al., 2008), ammonium nitrate mass fraction (ANMF) and acidity (Middlebrook et al., 2012). We installed a Nafion membrane dryer (Perma Pure MD) in front of the sampling inlet to minimise humidity effects on CE. In addition, more than 93.5% of data have an ANMF smaller than 0.4; only 6.5% of data would be influenced by a time dependent CE correction. Therefore, the ANMF did not significantly affect CE for this dataset. Nevertheless, **Fig. S1a** showed good agreements between the ACSM data corrected with a constant CE of 0.45 and the SO_4^{2-}, NO_3^-, and Cl^- anions from $PM_{2.5}$ filter samples (with R^2 of 0.83, 0.82, and 0.50, respectively). It also showed relatively good consistencies with the anions measured using chromatography from Mini-denuder (MD) (Dämmgen et al., 2010) samples (**Fig. S1b**). Besides, when adding the equivalent black carbon (eBC) concentration to the corrected ACSM data (CE=0.45), this reconstructed mass agreed well with external TEOM measurement of both $PM_{2.5}$ and PM_{10} daily mass concentrations with R^2 of 0.81 and 0.67, respectively (**Fig. S1c**). In addition, it (CE=0.45) had a slightly better correlation and a slope closer to 1 to these external measurements than the time-dependent CE corrected data as suggested by Middlebrook et al. (2012). Therefore, we used a constant CE value of 0.45 to quantify ACSM data.

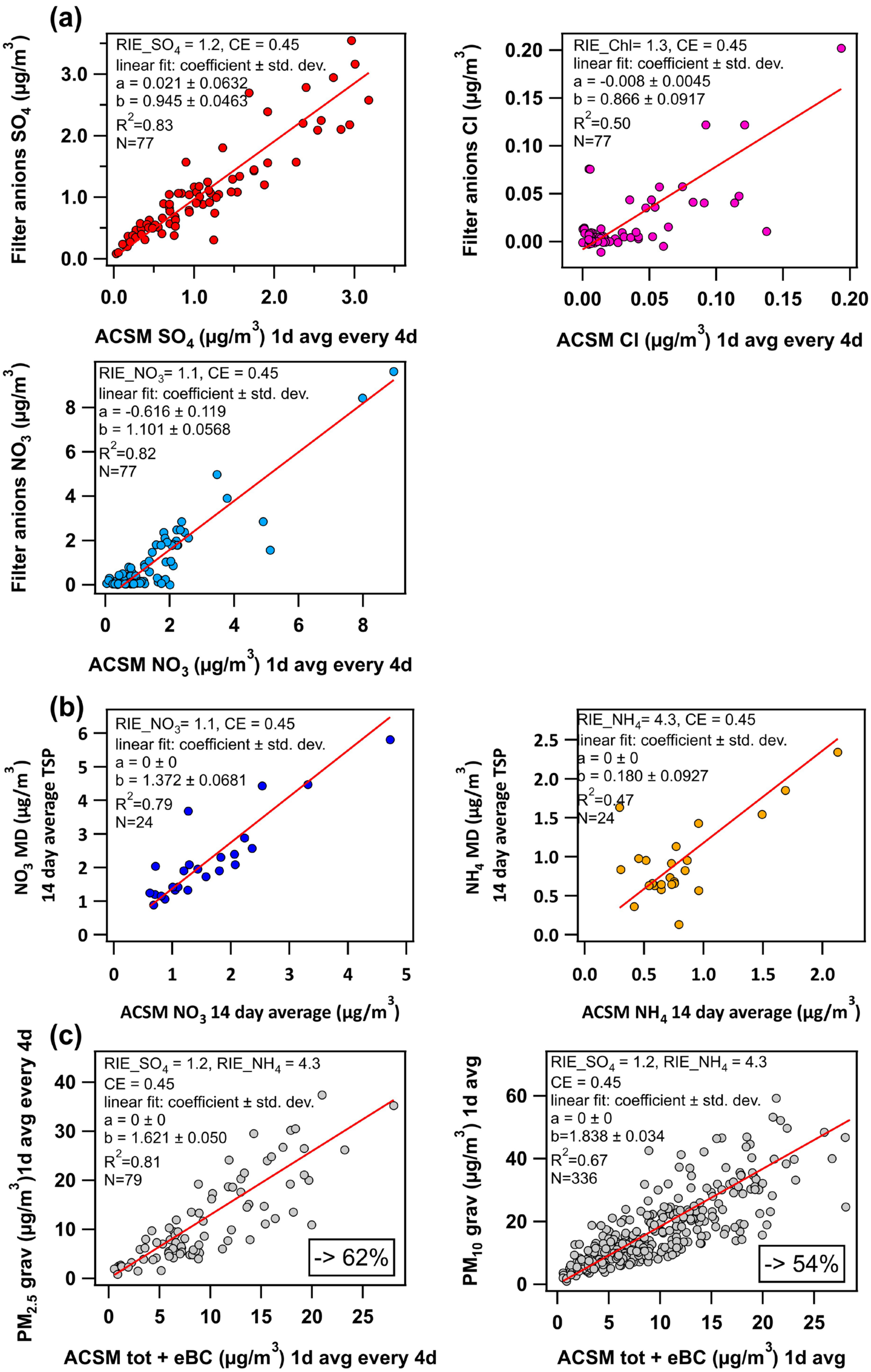
(a)
RIE_SO4 = 1.2, CE = 0.45
linear fit: coefficient ± std. dev.
a = 0.021 ± 0.0632
b = 0.945 ± 0.0463
R2=0.83
N=77
Filter anions SO4 (µg/m3)
ACSM SO4 (µg/m3) 1d avg every 4d
RIE_Chl= 1.3, CE = 0.45
linear fit: coefficient ± std. dev.
a = -0.008 ± 0.0045
b = 0.866 ± 0.0917
R2=0.50
N=77
Filter anions Cl (µg/m3)
ACSM Cl (µg/m3) 1d avg every 4d
RIE_NO3= 1.1, CE = 0.45
linear fit: coefficient ± std. dev.
a = -0.616 ± 0.119
b = 1.101 ± 0.0568
R2=0.82
N=77
Filter anions NO3 (µg/m3)
ACSM NO3 (µg/m3) 1d avg every 4d
(b)
RIE_NO3= 1.1, CE = 0.45
linear fit: coefficient ± std. dev.
a = 0 ± 0
b = 1.372 ± 0.0681
R2=0.79
N=24
NO3 MD (µg/m3)
14 day average TSP
ACSM NO3 14 day average (µg/m3)
RIE_NH4= 4.3, CE = 0.45
linear fit: coefficient ± std. dev.
a = 0 ± 0
b = 0.180 ± 0.0927
R2=0.47
N=24
NH4 MD (µg/m3)
14 day average TSP
ACSM NH4 14 day average (µg/m3)
(c)
RIE_SO4 = 1.2, RIE_NH4 = 4.3
CE = 0.45
linear fit: coefficient ± std. dev.
a = 0 ± 0
b = 1.621 ± 0.050
R2=0.81
N=79
-> 62%
PM2.5 grav (µg/m3)1d avg every 4d
ACSM tot + eBC (µg/m3) 1d avg every 4d
RIE_SO4 = 1.2, RIE_NH4 = 4.3
CE = 0.45
linear fit: coefficient ± std. dev.
a = 0 ± 0
b=1.838 ± 0.034
R2=0.67
N=336
-> 54%
PM10 grav (µg/m3) 1d avg
ACSM tot + eBC (µg/m3) 1d avg

Fig. S1 Mass closure analysis of the dataset. (a) Linear correlations between the filter anions SO_4^{2-}, NO_3^- and Cl^- and the corresponding ASCM inorganic species. (b) Correlations of the NO_3^- and NH_4^+ concentrations measured with mini-denuders and by the ACSM. (c) Correlations of $PM_{2.5}$ and PM_{10} with NR-PM_1 defined as the sum of the total ACSM mass plus the equivalent black carbon concentration.

S2 Black carbon measurement and source apportionment

The aethalometer (AE 31 model by Magee Scientific Inc.) measures equivalent black carbon (eBC) concentrations via light transmission through a sample spot at multiple wavelengths (λ = 370, 470, 520, 590, 660, 880, and 950 nm). In this study, we installed a $PM_{2.5}$ cyclone and a Nafion dryer (Perma Pure MD) in front of the sampling inlet that the AE31 and the ACSM shared. The light absorption coefficients b_{abs} were calculated by correcting the measured attenuation coefficients for the filter loading effect (Weingartner et al., 2003). To convert the optical absorption to the eBC mass concentration, eBC_{tot} into µg m^{-3} (Petzold et al., 2013), the absorption coefficient at a given wavelength λ, $b_{abs}(\lambda)$ was divided by the corresponding aerosol mass absorption cross-section $\sigma_{abs}(\lambda)$ in m^2 g^{-1} (Weingartner et al., 2003):

$$eBC_{tot} = b_{abs}(\lambda)/\sigma_{abs}(\lambda) \qquad \textit{(1)}$$

with $\sigma_{abs}(470)$ = 22.9 m^2 g^{-1} and $\sigma_{abs}(950)$ = 8.8 m^2 g^{-1}, as previously reported for Magadino (Herich et al., 2011).

The light absorption coefficients measured at wavelengths λ_1 = 470 nm and λ_2 = 950 nm were used to retrieve the relative contributions of traffic (eBC_{tr}) and wood burning (eBC_{wb}) to the total equivalent black carbon mass concentration eBC_{tot} (Herich et al., 2011; Sandradewi et al., 2008; Zotter et al., 2017). The two-component model implies that at a given wavelength λ the absorption coefficient b_{abs} is approximated by the sum of the absorption coefficients of eBC emitted from traffic exhaust $b_{abs,tr}$ and from wood burning $b_{abs,wb}$ (Eq. (2)), which in turn depend on λ through Eq. (3) and Eq.(4):

$$b_{abs}(\lambda) = b_{abs,tr}(\lambda) + b_{abs,tr}(\lambda) \tag{2}$$

$$\frac{b_{abs,tr}(\lambda_1)}{b_{abs,tr}(\lambda_2)} = (\frac{\lambda_1}{\lambda_2})^{-\alpha_{tr}} \tag{3}$$

$$\frac{b_{abs,wb}(\lambda_1)}{b_{abs,wb}(\lambda_2)} = (\frac{\lambda_1}{\lambda_2})^{-\alpha_{wb}} \tag{4}$$

The Ångstrom exponents for eBC from traffic $\alpha_{tr} = 0.9$ and wood burning $\alpha_{wb} = 1.68$ sources were chosen in accordance with Zotter et al. (2017) suggested for the same sampling site, Magadino.

Note that despite of utilising the aethalometer corrections proposed in Weingartner et al. (2003), the eBC data were not fully free of filter loading artefacts, as evidenced by a discontinuity in $b_{abs}(\lambda)$ measurements on filter tape advancement. Since the filter loading effect is more pronounced at shorter wavelengths due to higher attenuation (Drinovec et al., 2015; Weingartner et al., 2003), b_{abs} measured at 470nm will have more intense signals. As a result, when high eBC loadings triggered more frequent filter advances for winter days, artificial peaks appeared in the time series of apportioned eBC_{wb}. However, when averaging data points for the eBC diurnal cycles that we used to validate positive matrix factorisation (PMF) solutions, transient peaks due to the filter loading artefacts had negligible effects.

S3 Rolling PMF analysis

S3.1 Factor analysis of the organic mass spectra

PMF has been demonstrated to be a useful tool to retrieve the sources of measured organic aerosol mass spectra with a bilinear factor model (Paatero and Tapper, 1994; Ulbrich et al., 2009):

$$x_{ij} = \sum_{k=1}^{p} g_{ik} \times f_{kj} + e_{ij} \tag{5}$$

where x_{ij} is the mass concentration of the j^{th} mass spectral variable in the time point i^{th}; g_{ik} is the contribution of the k^{th} factor in the i^{th} time point; f_{kj} is the concentration of the j^{th} mass spectral variable in the k^{th} factor; and e_{ij} is the residual of j^{th} variable of the mass spectra in i^{th} time point. The superscript, p represents the number of factors, which the user determines. The cost function of PMF uses least-squares algorithm by iteratively minimising the following quantity Q:

$$Q = \sum_{i=1}^{n} \sum_{j=1}^{m} (\frac{e_{ij}}{\sigma_{ij}})^2 \tag{6}$$

where σ_{ij} is an element in the $n \times m$ matrix of the measurement uncertainties, which corresponds point-by-point to x_{ij}. In addition, we normalised the quantity $\frac{Q}{Q_{exp}}$ as a mathematical metric during PMF analysis, where the Q_{exp} is:

$$Q_{\text{exp}} = (n \times m) - p \times (n + m) \tag{7}$$

The $\frac{Q}{Q_{exp}}$ supports the user to determine the number of factors required for the model by investigating the effects on this quantity of adding/removing a factor. However, PMF itself suffers from rotational ambiguity because the object function, Q does not provide unique solutions, that is, when $\mathbf{G} \cdot \mathbf{F} = \mathbf{G} \cdot \mathbf{T} \cdot \mathbf{T}^{-1} \cdot \mathbf{F}$, PMF provides a similar value of Q but very different solutions (rotated matrix $\overline{\mathbf{G}} = \mathbf{G} \cdot \mathbf{T}$ (rotated factor time series) and $\overline{\mathbf{F}} = \mathbf{T}^{-1} \cdot \mathbf{F}$ (rotated factor profiles)). Only one or even none of these rotated solutions may be atmospherically relevant. The ME-2 solver (Paatero, 1999) enables theoretically complete rotational control over the factor solutions, which is implanted here by imposing constraints via the *a*-value approach on one or more elements of **F** and/or **G** (Paatero and Hopke, 2009). The *a*-value (ranging from 0 to 1) determines how much the resulting factor ($f_{j,solution}$) or time series ($g_{j,solution}$) can vary from the input reference factor ($f_{j,reference}$) or time series ($g_{j,reference}$) as shown in Eq.(8) and Eq.(9):

$$f_{j,solution} = f_{j,reference} \pm a \cdot f_{j,reference} \tag{8}$$

$$g_{j,solution} = g_{j,reference} \pm a \cdot g_{j,reference} \tag{9}$$

Previous work using *a*-values has shown to retrieve environmentally reasonable PMF solutions efficiently. The presence of legitimate *a priori* constraints decrease the degree of rotational ambiguity (Canonaco et al., 2013, 2021; Crippa et al., 2014; Lanz et al., 2008). Here we configured the ME-2 solver and analysed PMF results using SoFi (Source Finder, Datalystica Ltd., Villigen, Switzerland) Pro 6.D interface (Canonaco et al., 2013, 2021), developed within the IGOR Pro software (WaveMetrics Inc., Lake Oswego, OR, USA).

S3.2 Preparations and settings for Rolling PMF with ME-2

S3.2.1 Seasonal PMF *pre-tests*

To understand the potential sources over different seasons in Magadino, PMF *pre-tests* were conducted based on different seasons. It provides information about the potential number of factors in different seasons, which is necessary before the rolling PMF analysis. In addition, the PMF solutions from rolling PMF analysis tend to be more robust if the reference profiles used to constrain are retrieved from seasonal PMF analysis. Thus, site-dependent reference profiles are necessary (at least for BBOA) to get more accurate estimations of OA sources (i.e., better correlation with external tracers in this study compared to the PMF solution using literature reference profiles). In this study, the whole dataset was divided into five parts based on months (i.e., DJF represents the winter season during December, January, and February; MAM represents the spring season during March, April, and May, etc.). A preliminary "good" PMF solution (so-called base case) can be obtained for each season by following the guidelines provided by Crippa et al. (2014).

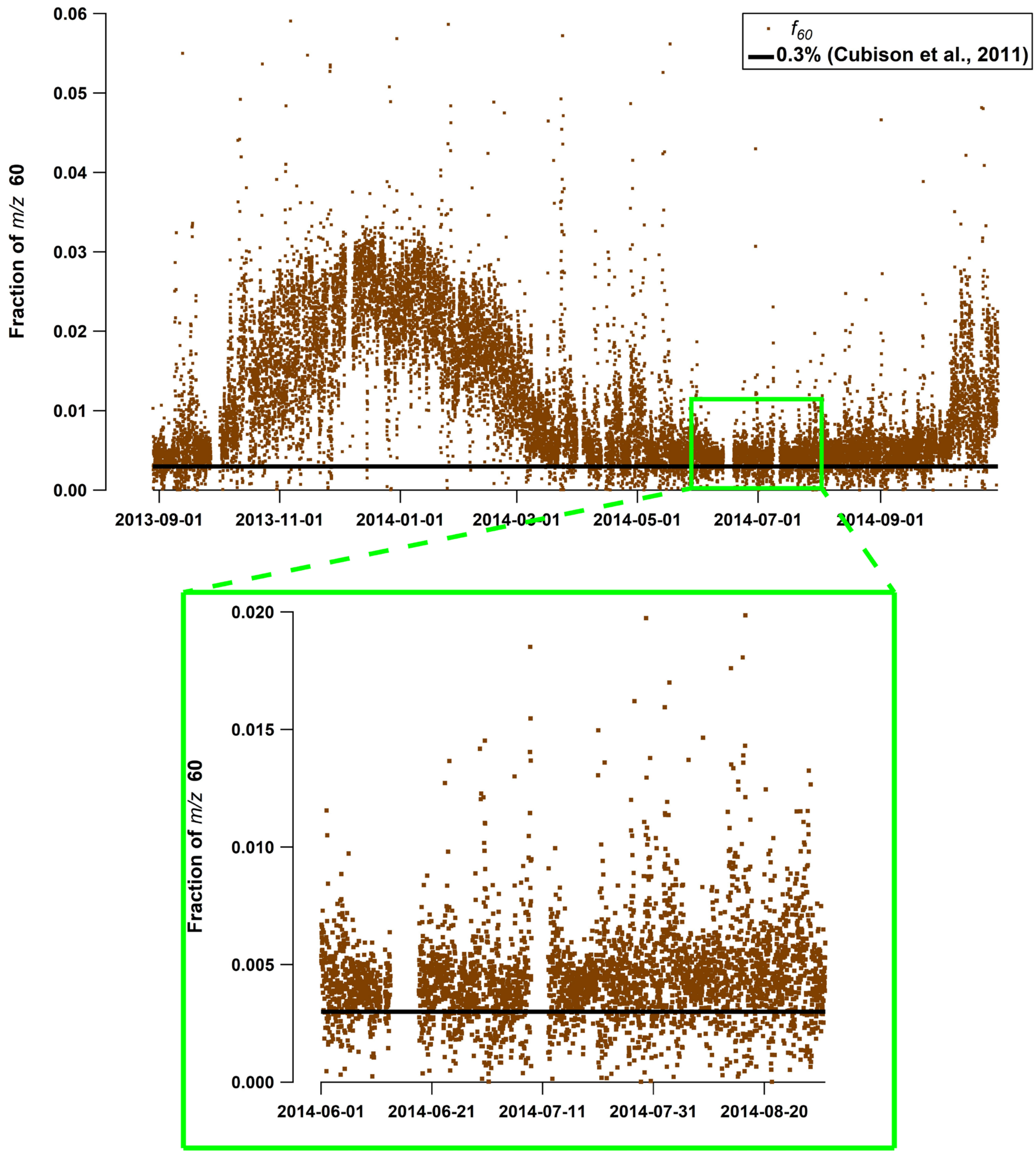

Fig. S2 Time series of the measured fraction of mass-to-charge ratio (*m/z*) of 60 .

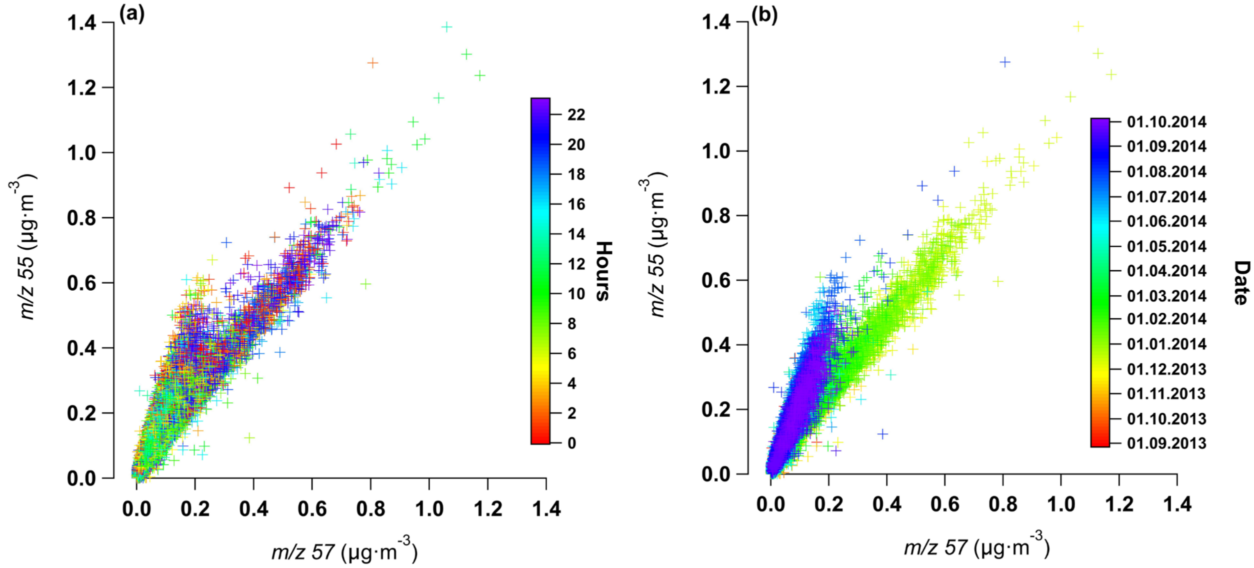

Fig. S3 Measured absolute mass concentrations of *mass-to-charge ratio (m/z)*=55 and *m/z*=57 with colour coded by hours of the day (a) and date and time (b).

S3.2.2 Bootstrap seasonal PMF analysis

In order to get stable reference profiles, the bootstrap resampling technique was applied in this study to test the stability of the base cases from seasonal PMF *pre-tests*. The bootstrap resampling randomly chooses a subset of the original matrix and replicates some rows/columns to create a new matrix with the same size (Efron, 1979). Given sufficient bootstrapped runs (>100) can provide the statistical uncertainty of the PMF solutions.

First, the primary factor profiles (hydrocarbon-like OA factor (HOA), BBOA) were retrieved from preliminary tests during seasonal PMF runs, while an additional mass-to-charge ratio (*m/z*) 58 related OA (58-OA) factor was obtained in summer, then 1000 PMF runs were conducted for each season by constraining the POA factor profiles using random *a*-values with a step of 0.1 and ranging from 0 to 0.5. We used the same criterion list as the base case (as shown in **Table S1**) and a novel technique, *t*-test (Section 3.3) to define "good" PMF runs. Then, from the averaged bootstrapped PMF solutions (**Fig. S4**), the reference profiles can be obtained for rolling PMF analysis.

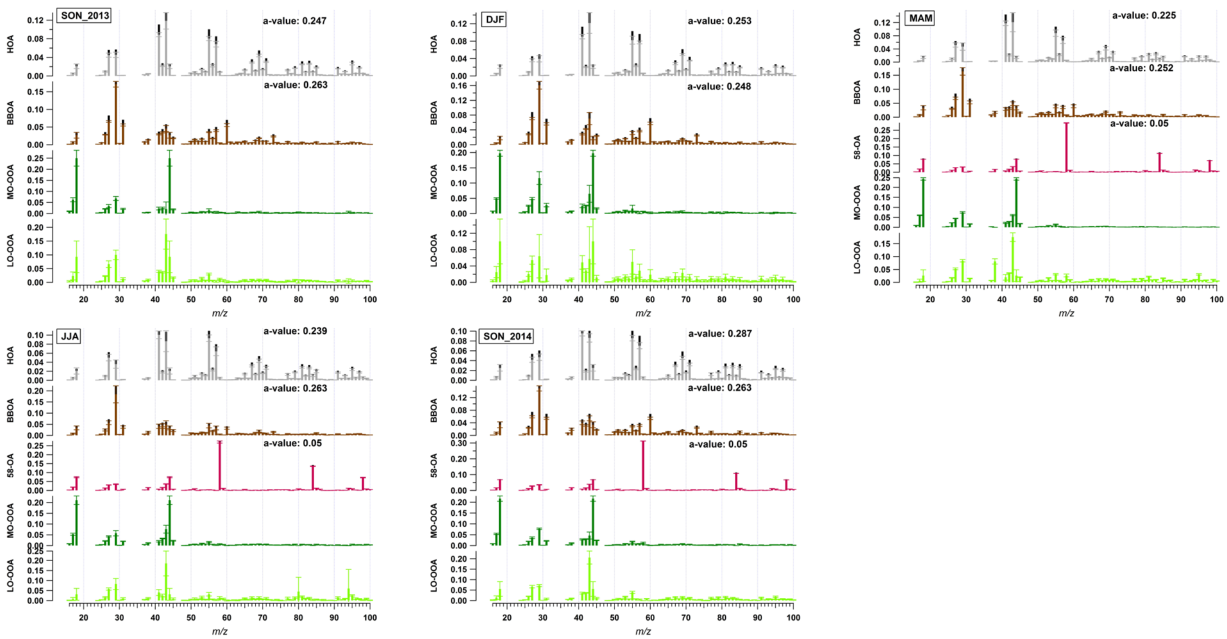

Fig. S4 Averaged factor profiles from seasonal bootstrap solutions for five different periods. The error bars of each factor represent the standard deviation of the averaged bootstrapped solution, the thick dark sticks are the variabilities that each variable allowed to vary with the corresponding averaged *a*-value. SON = September, October and November, DJF = December, January and February, MAM = March, April, and May, JJA = June, July, and August.

S3.2.3 PMF Window settings

In order to retrieve appropriate constraints, we performed PMF *pre-tests* and bootstrap analysis for different seasons. Here, we constrained primary OA factor profiles (hydrocarbon-like OA (HOA) and biomass burning OA (BBOA)) as well as the factor profile of the 58-OA using the *a*-value technique in the rolling PMF analysis. The reference profiles of HOA and BBOA were from the winter bootstrapped PMF solution (December, January, and February), as shown in **Fig. S4**. With a higher contribution of the biomass burning trace ion *m/z* 60 in the winter, we expect a more representative and robust BBOA profile from the winter solution than from the other seasons. The 58-OA profile was retrieved from the summer bootstrapped PMF solution (June, July, and August) (**Fig. S4**). To allow the factor profile to adapt itself over time, we applied an *a*-value randomly from a set of *a*-values, including 0, 0.1, 0.2, 0.3, and 0.4 (so-called random *a*-value approach). Canonaco et al. (2021) suggested that an upper *a*-value of 0.4 is sufficient to cover the temporal variation of OA source profiles. Moreover, due to the uniqueness of the 58-OA chemical profile, it was tightly constrained with a constant *a*-value of 0.05.

In total, we constrained the HOA and BBOA factors with a random *a*-value (0–0.4, with a step of 0.1) and an exact *a*-value (0.05) for the 58-OA factor in the rolling PMF analysis. There are 25 (5×5) possible *a*-value combinations within an individual rolling window. Therefore, 50 PMF iterations for each time window are sufficient to cover all possibilities of the *a*-value combinations. With the rolling window of 50 repeats, each data point (except the data within the first and last time window) will actually have many PMF iterations (i.e., length of the window×50), where bootstrap resampling and random combinations of constraints is performed. It allows to estimate the statistical and rotational uncertainties of the PMF factors (Canonaco et al., 2021). To find the optimum length of the time windows, we tested four different lengths of the time windows (1, 7, 14, and 28 days) using the same approaches as in Canonaco et al. (2021). We determined the optimum length of the time window based on the number of missing data points (un-modelled data due to the selection based on the criteria) while applying the same thresholds for the same criteria.

S3.2.4 Criteria settings

Performing a rolling analysis for one-year data with 50 repeats per window requires tens of thousands of PMF runs. Manual inspection of all PMF runs is impractical and therefore was replaced by monitoring user-defined criterion scores (Canonaco et al., 2021). In this study, R^2 values of the time series of modelled HOA vs NO_x and eBC_{tr} were used for HOA. The BBOA factor was inspected using the variation of *m/z*=60 explained by BBOA (**Table S1**). For these time series based criteria (criterion 1 to criterion 3 in **Table S1**), we deployed a student *t*-test to minimise subjective judgments while determining the thresholds (more discussions in Section 3.3 of this document).

Typically, OOA factors are dominated by the signals of f_{43} ($C_2H_3O^+$ at *m/z* = 43) and f_{44} (CO_2^+ at *m/z* = 44) that correspond to the less and more oxygenated ion fragments (Crippa et al., 2014; Ng et al., 2010), where *f* is the fraction of a variable, *i.e.* the intensity $I_{m/z}$ normalised by the sum of the intensities of all organic *m/z* variables. In this study, we were able to retrieve two OOA factors (i.e., more oxidised OOA (MO-OOA) and less oxidised OOA (LO-OOA)) for the whole year. Since we left two factors unconstrained (4^{th} and 5^{th} factor), MO-OOA can be either at the 4^{th} or the 5^{th} position in these 20750 runs. Thus, we used the f_{44} for the 4^{th} factor to sort the unconstrained OOA factors to ensure MO-OOA and LO-OOA sitting on the 4^{th} and the 5^{th} position, respectively. The details of the sorting scheme can be found in Canonaco et al. (2021). At the same time, we also monitored f_{43} in LO-OOA and f_{44} in MO-OOA to make sure they are not zero. With this set of criteria, we were able to only select "good" (atmospherically relevant) PMF runs before averaging.

S3.2.4.1Explained variation (EV) of m/z = 60 by BBOA

The uncertainties of the aethalometer model for eBC source apportionment are very high when the mass concentration of eBC_{wb} is small (Harrison et al., 2013), which was the case in summer 2014. Thus, the summer BBOA factor was poorly correlated with eBC_{wb}. In this work, we used the variation of m/z = 60 explained by BBOA to justify the summer solution, which is calculated using Eq. (10) (Paatero, 2010):

$$EV_{j,k} = \frac{\sum_{i=1}^{n}\left(\left|g_{ik}\cdot f_{kj}\right|/\sigma_{ij}\right)}{\sum_{i=1}^{n}\left(\left(\sum_{h=1}^{p}\left|g_{ih}\cdot f_{hj}\right| + e_{ij}\right)/\sigma_{ij}\right)} \qquad \textbf{(10)}$$

Paatero (2010) suggested that if there is a dominant ion in a specific factor, it should explain more than 30-35% of variation of this measured variable. Canonaco et al. (2021) used an EV of 0.25 at m/z=60 for BBOA as a threshold to select "good" runs for BBOA. In this study, we only selected PMF runs with EV of m/z=60 for BBOA that were significantly larger than those of other factors by t-test with a p-value ≤ 0.05. In the end, the $EV_{60,BBOA}$ values for selected PMF runs for both seasonal and rolling results are all larger than 0.4.

Table S1 Criterion List for both seasonal and rolling PMF.

	Criterion	**Type**	**Threshold**
1	**HOA vs NO_x**	$R^2_{pearson}$, normal time series	p-value ≤ 0.05
2	**HOA vs eBC_{tr}**	$R^2_{pearson}$, normal time series	p-value ≤ 0.05
3	$\boldsymbol{EV_{60,BBOA}}$	Average, normal time series	p-value ≤ 0.05
4	**factor_4[44]**	Profiles, fraction, **sorting criterion**	>0
5	**factor_5[43]**	Profiles, fraction	>0

S3.3 Definition of "good" PMF runs using the *t*-test

The conventional PMF analysis remains subjective on how to define "good" (environmentally reasonable) PMF runs. In this study, we tried to use the criteria-based approach to have a quantitative analysis (e.g., correlations between the time series of a PMF factor and corresponding external tracers, intensities of key ions of the PMF factor profile) on all PMF runs as suggested by Canonaco et al. (2021). However, it is still subjective to decide the lower limit for "good" PMF runs, as Canonaco et al. (2021) suggested.

Canonaco et al. (2021) proposed to define thresholds of criteria for the rolling PMF runs based on the seasonal PMF analysis. For instance, for the criterion of the R^2-Pearson between NO_x vs HOA, SoFi Pro can resample the time series of both the BBOA factor (from averaged seasonal bootstrapped solutions) and NO_x by bootstrap. It then uses the resampled time series to conduct correlation analysis, which provides systematic statistic metrics, including mean, median, minimum, maximum, and $10^{th}/90^{th}$ percentile, probability distribution function, etc. Canonaco et al. (2021) proposed to use the 10^{th} percentile as the lower limit of the criteria in the rolling PMF analysis. However, it remains subjective when the user defines the thresholds for the "good" seasonal solutions. In addition, there could also be a dilemma when the thresholds are too strict to allow sufficient data coverage in the end. As shown in **Fig. S5a**, the 10^{th} percentile (R^2=0.438) caused a high rejection rate for the majority of data points in fall 2013. This is potentially due to the fact that the resampling size for the seasonal solution during bootstrap of criteria is not small enough, therefore, the resampled correlations appeared to be not representative for the rolling solution.

In this study, we proposed a new technique to minimise subjective judgements from the user. We use the student *t*-test with the null hypothesis of un-correlation between the two variables (e.g., R^2 of the time series of modelled HOA vs NO_x). For other typical criteria that are based on temporal information (e.g., explained variation of *m/z* = 60 for BBOA), we used the null hypothesis of $EV_{60,BBOA}$ being not larger than EV_{60} of all other factors. With these *t*-tests, we utilised the *p*-value to filter out "bad" PMF runs. The statistical significance level of a *p*-value $\leq$ 0.05 was applied for criterion 1, 2, and 3 (**Table S1**) to define "good" solutions with minimum subjective judgements. In addition, compared with the 10^{th} percentile technique Canonaco et al. (2021) proposed, the *t*-test approach typically would accept more data points as illustrated in **Fig. S5b**.

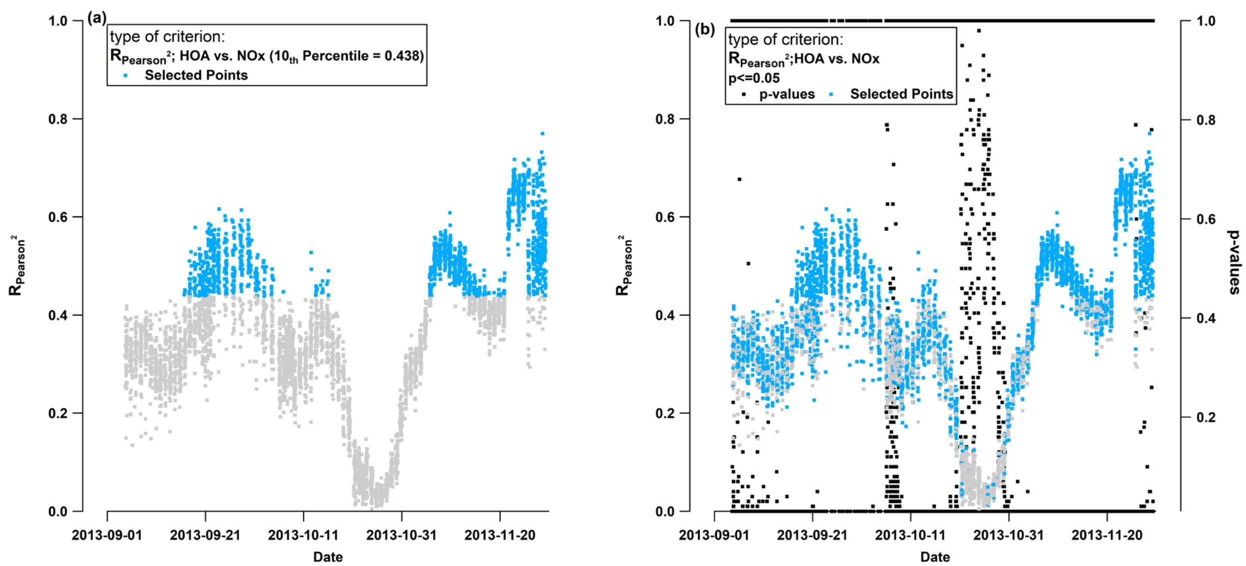

Fig. S5 Score plot the criterion for the R^2 of HOA vs NO_x in rolling PMF for fall, 2013.

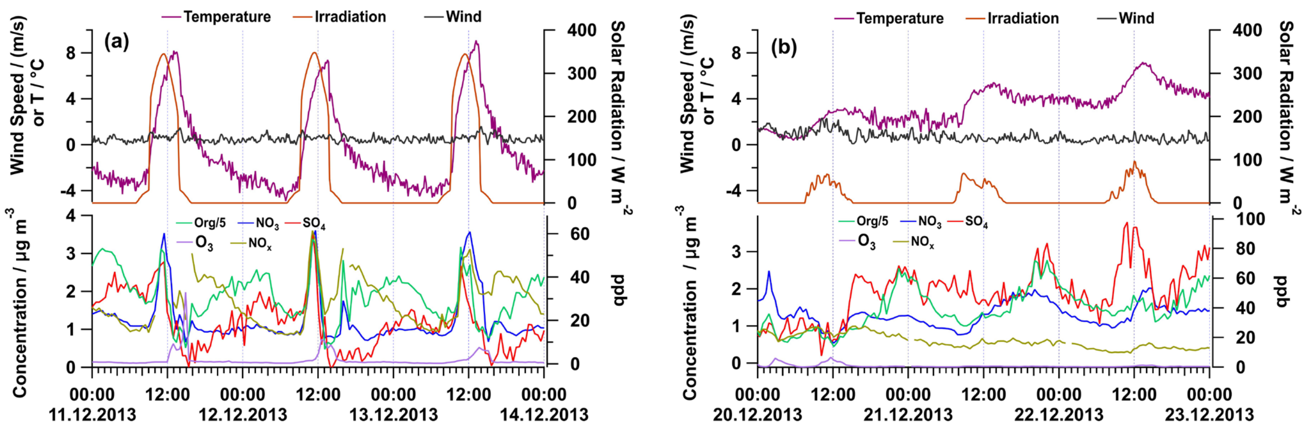

Fig. S6 Diurnal cycles of the organic (Org), NO_3, SO_4, O_3, NO_x, and corresponding meteorological data on sunny (a) and cloudy (b) days in winter. On sunny days (a), a transport phenomenon was observed in the noontime which caused a sharp enhancement of pollutants, followed by a breakthrough of the boundary layer resulting in simultaneous dilution for all pollutants. Also, the delay of the irradiation peak is because the monitoring station lies in the shadow of surrounding mountains during the winter season. (b) No such situation was observed during cloudy days which indicates that indeed irradiation and temperature gradient might play a role in this phenomenon.

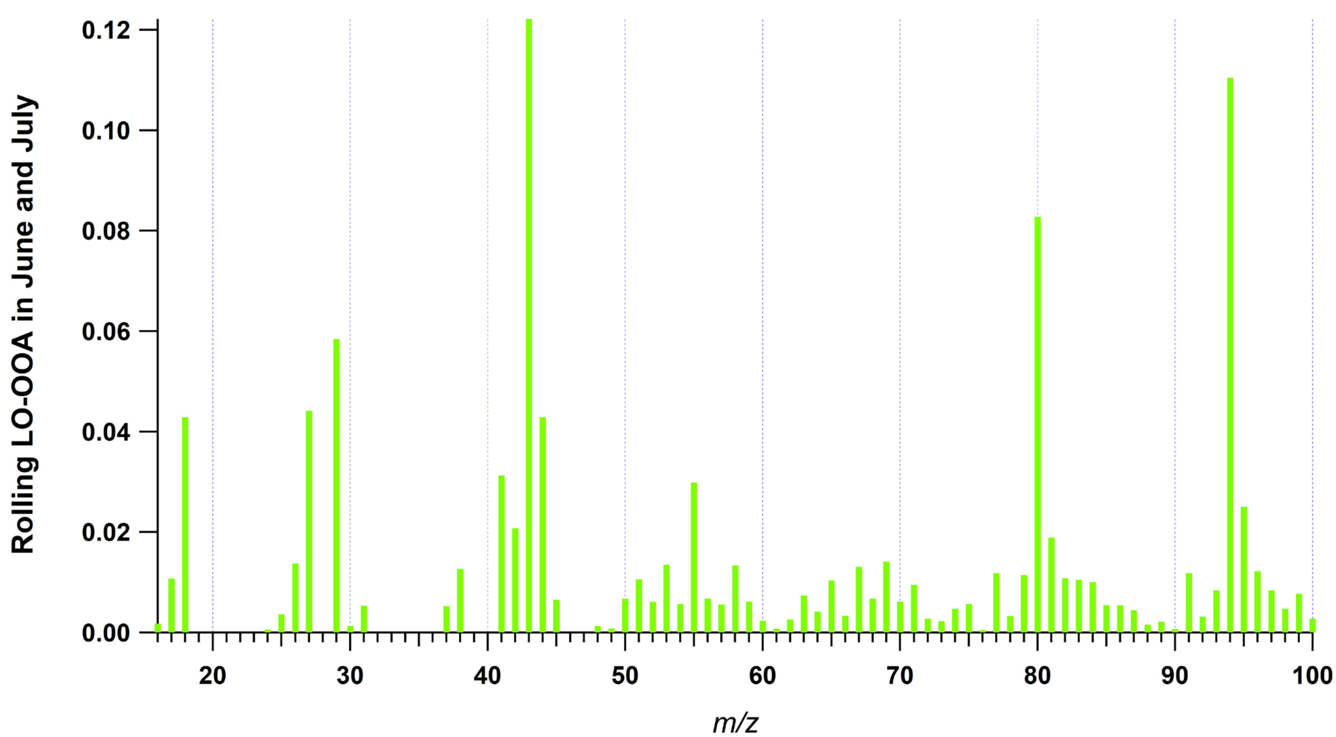

Fig. S7 Mass spectra for LO-OOA in June and July from the rolling results.

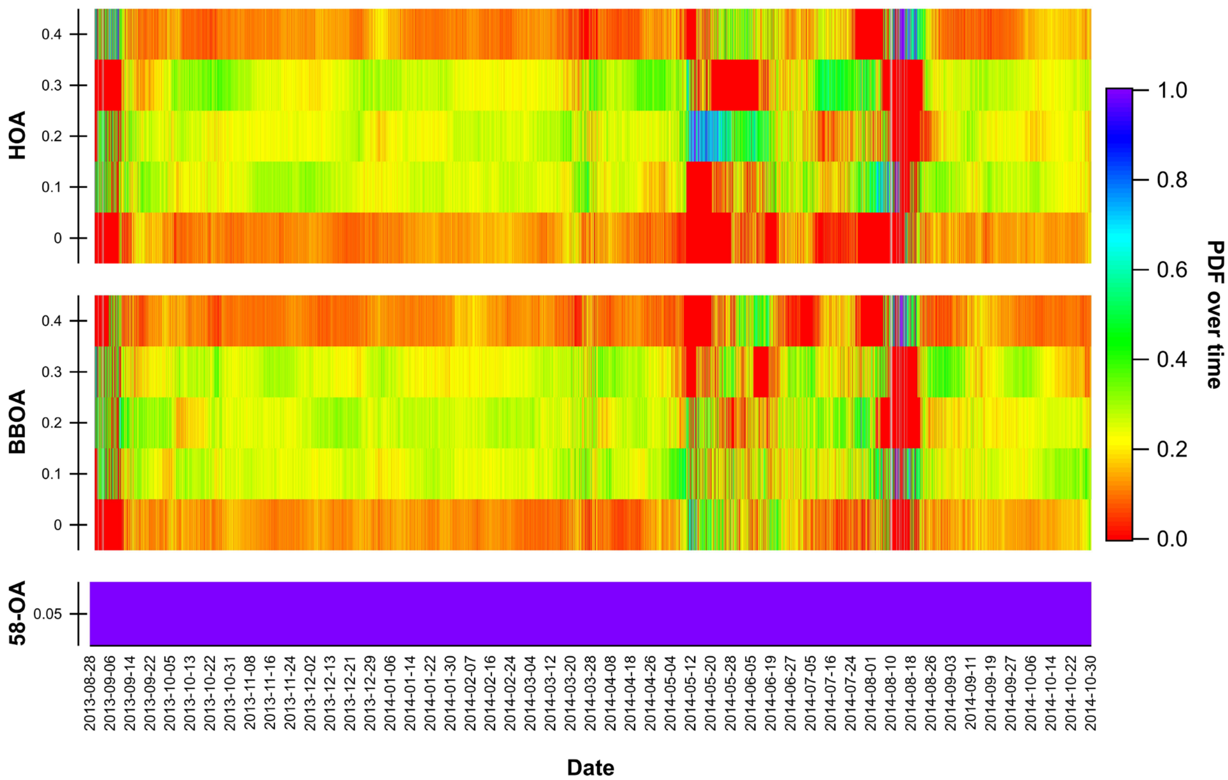

Fig. S8 The probability distribution function (PDF) of employed *a*-values of selected PMF runs for constrained factors as a function of time.

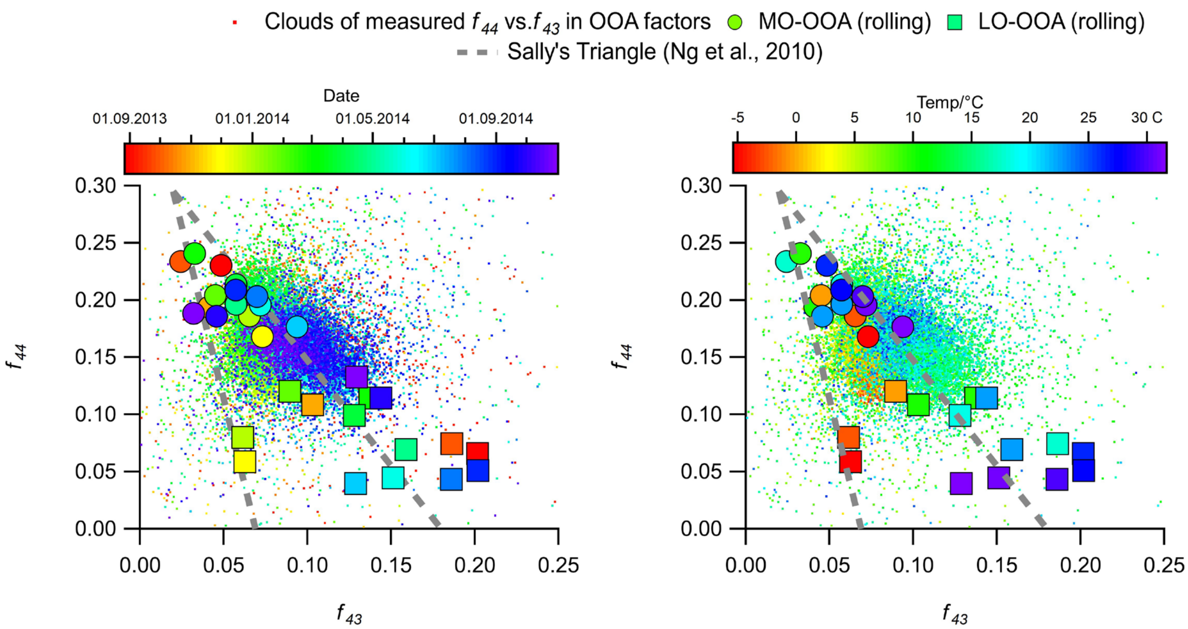

Fig. S 9 f_{44} vs. f_{43} for OOA factors (after subtraction of signals contributed by the primary HOA, BBOA and 58-OA factors as shown in Eq. (S11) and (S12)) in monthly resolution, colour coded by month (left) and temperature (right).

$$subtracted\ f_{44} = \frac{mass\ conc.\ of\ OOA\ @[m/z\ 44]}{mass\ conc.\ of\ OOA + residual\ of\ total\ OA} \quad \textbf{(11)}$$

$$subtracted\ f_{43} = \frac{mass\ conc.\ of\ OOA\ @[m/z\ 43]}{mass\ conc.\ of\ OOA + residual\ of\ total\ OA} \quad \textbf{(12)}$$

S4 Optimised time window size

We tested different time window size (1, 7, 14, and 28 days) and compared the solutions by applying the same thresholds for the same criteria. We found the optimum window sizes for this dataset to be 14 days, with only 29 (0.15%) non-modelled points (due to the criteria-based selection) as shown in **Fig. S10**. The averaged Q/Q_{exp} for different time window sizes are similar, but the 14-day window solution still has the smallest Q/Q_{exp} (0.448). However, the Q/Q_{exp} for all window sizes are smaller than one, which is likely due to the high uncertainty from the measurement of the ACSM (27/67 variables have signal to noise ratio (*S/N*) <2), and SoFi simplifies the equation of Q_{exp} to n×m because n×m >> p×(n+m) when measured points are sufficiently large. Nevertheless, we selected and presented the 14-day window solution in this manuscript with its significantly smaller number of missing (non-modelled) points in the model.

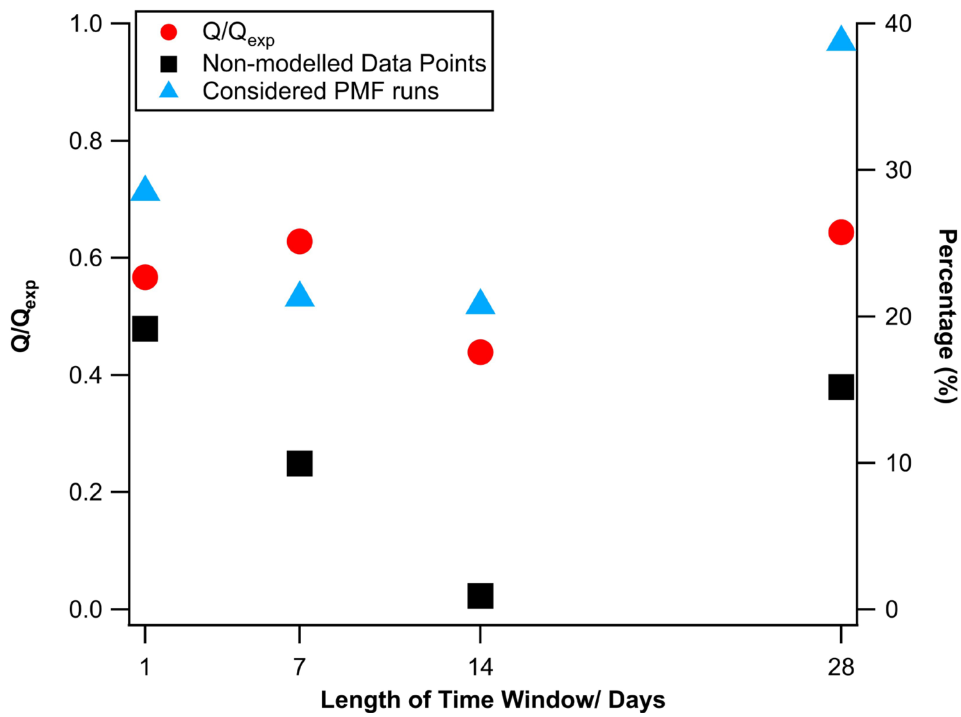

Fig. S10 Non-modelled time points (due to criteria-based selection) and Q/Q_{exp} vs rolling window size.

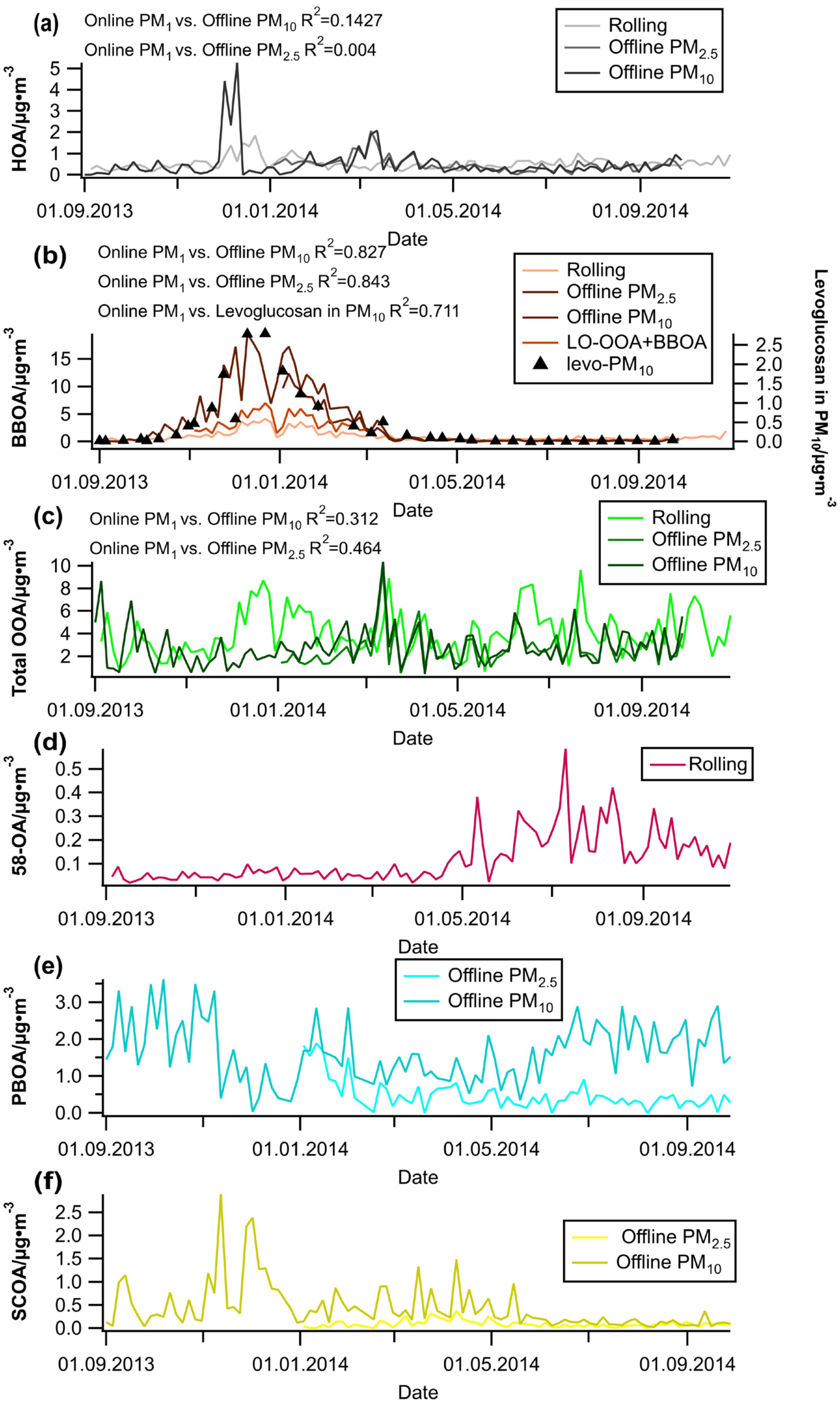

Fig. S11 The comparison between source apportionment results from offline AMS PM_{10}/$PM_{2.5}$ samples and online ACSM.

References

Canonaco, F., Crippa, M., Slowik, J. G., Baltensperger, U. and Prévôt, A. S. H. H.: SoFi, an IGOR-based interface for the efficient use of the generalized multilinear engine (ME-2) for the source apportionment: ME-2 application to aerosol mass spectrometer data, Atmos. Meas. Tech., 6(12), 3649–3661, doi:10.5194/amt-6-3649-2013, 2013.

Canonaco, F., Tobler, A., Chen, G., Sosedova, Y., Slowik, J. G., Bozzetti, C., Daellenbach, K. R., El Haddad, I., Crippa, M., Huang, R.-J., Furger, M., Baltensperger, U. and Prévôt, A. S. H.: A new method for long-term source apportionment with time-dependent factor profiles and uncertainty assessment using SoFi Pro: application to 1 year of organic aerosol data, Atmos. Meas. Tech., 14(2), 923–943, doi:10.5194/amt-14-923-2021, 2021.

Crippa, M., Canonaco, F., Lanz, V. A., Äijälä, M., Allan, J. D., Carbone, S., Capes, G., Ceburnis, D., Dall'Osto, M., Day, D. A., DeCarlo, P. F., Ehn, M., Eriksson, A., Freney, E., Hildebrandt Ruiz, L., Hillamo, R., Jimenez, J. L., Junninen, H., Kiendler-Scharr, A., Kortelainen, A.-M. M., Kulmala, M., Laaksonen, A., Mensah, A. A., Mohr, C., Nemitz, E., O'Dowd, C., Ovadnevaite, J., Pandis, S. N., Petäjä, T., Poulain, L., Saarikoski, S., Sellegri, K., Swietlicki, E., Tiitta, P., Worsnop, D. R., Baltensperger, U., Prévôt, A. S. H. H., Dall'Osto, M., Day, D. A., DeCarlo, P. F., Ehn, M., Eriksson, A., Freney, E., Hildebrandt Ruiz, L., Hillamo, R., Jimenez, J. L., Junninen, H., Kiendler-Scharr, A., Kortelainen, A.-M. M., Kulmala, M., Laaksonen, A., Mensah, A. A., Mohr, C., Nemitz, E., O'Dowd, C., Ovadnevaite, J., Pandis, S. N., Petäjä, T., Poulain, L., Saarikoski, S., Sellegri, K., Swietlicki, E., Tiitta, P., Worsnop, D. R., Baltensperger, U. and Prévôt, A. S. H. H.: Organic aerosol components derived from 25 AMS data sets across Europe using a consistent ME-2 based source apportionment approach, Atmos. Chem. Phys., 14(12), 6159–6176, doi:10.5194/acp-14-6159-2014, 2014.

Dämmgen, U., Thöni, L., Lumpp, R., Gilke, K., Seitler, E. and Bullinger, M.: Feldexperiment zum Methoden- vergleich von Ammoniak- und messungen in der Umgebungsluft , 2005 bis 2008 in Braunschweig, vTI Agric. For. Res. - Sonderh., (337), 62 [online] Available from: https://www.thuenen.de/media/publikationen/landbauforschung-sonderhefte/lbf_sh337.pdf, 2010.

Drinovec, L., Močnik, G., Zotter, P., Prévôt, A. S. H. H., Ruckstuhl, C., Coz, E., Rupakheti, M., Sciare, J., Müller, T., Wiedensohler, A. and Hansen, A. D. A. A.: The "dual-spot" Aethalometer: an improved measurement of aerosol black carbon with real-time loading compensation, Atmos. Meas. Tech., 8(5), 1965–1979, doi:10.5194/amt-8-1965-2015, 2015.

Efron, B.: Bootstrap Methods: Another Look at the Jackknife, Ann. Stat., 7(1), 1–26 [online] Available from: https://www.jstor.org/stable/2958830, 1979.

Harrison, R. M., Beddows, D. C. S., Jones, A. M., Calvo, A., Alves, C. and Pio, C.: An evaluation of some issues regarding the use of aethalometers to measure woodsmoke concentrations, Atmos. Environ., 80, 540–548, doi:10.1016/j.atmosenv.2013.08.026, 2013.

Herich, H., Hueglin, C. and Buchmann, B.: A 2.5 year's source apportionment study of black carbon from wood burning and fossil fuel combustion at urban and rural sites in Switzerland, Atmos. Meas. Tech., 4(7), 1409–1420, doi:10.5194/amt-4-1409-2011, 2011.

Lanz, V. A., Alfarra, M. R., Baltensperger, U., Buchmann, B., Hueglin, C., Szidat, S., Wehrli, M. N., Wacker, L., Weimer, S., Caseiro, A., Puxbaum, H. and Prevot, A. S. H.: Source Attribution of Submicron Organic Aerosols during Wintertime Inversions by Advanced Factor Analysis of Aerosol Mass Spectra, Environ. Sci. Technol., 42(1), 214–220, doi:10.1021/es0707207, 2008.

Matthew, B. M., Middlebrook, A. M. and Onasch, T. B.: Collection Efficiencies in an Aerodyne Aerosol Mass Spectrometer as a Function of Particle Phase for Laboratory Generated Aerosols, Aerosol Sci. Technol., 42(11), 884–898, doi:10.1080/02786820802356797, 2008.

Middlebrook, A. M., Bahreini, R., Jimenez, J. L. and Canagaratna, M. R.: Evaluation of Composition-Dependent Collection Efficiencies for the Aerodyne Aerosol Mass Spectrometer using Field Data, Aerosol Sci. Technol., 46(3), 258–271, doi:10.1080/02786826.2011.620041, 2012.

Ng, N. L., Canagaratna, M. R., Zhang, Q., Jimenez, J. L., Tian, J., Ulbrich, I. M., Kroll, J. H., Docherty, K. S., Chhabra, P. S., Bahreini, R., Murphy, S. M., Seinfeld, J. H., Hildebrandt, L., Donahue, N. M., DeCarlo, P. F., Lanz, V. A., Prévôt, A. S. H. H., Dinar, E., Rudich, Y. and Worsnop, D. R.: Organic aerosol components observed in Northern Hemispheric datasets from Aerosol Mass Spectrometry, Atmos. Chem. Phys., 10(10), 4625–4641, doi:10.5194/acp-10-4625-2010, 2010.

Paatero, P.: The Multilinear Engine—A Table-Driven, Least Squares Program for Solving Multilinear Problems, Including the n -Way Parallel Factor Analysis Model, J. Comput. Graph. Stat., 8(4), 854–888, doi:10.1080/10618600.1999.10474853, 1999.

Paatero, P.: User's guide for positive matrix factorization programs PMF2 and PMF3, Helsinki, Finland., 2010.

Paatero, P. and Hopke, P. K.: Rotational tools for factor analytic models, J. Chemom., 23(2), 91–100, doi:10.1002/cem.1197, 2009.

Paatero, P. and Tapper, U.: Positive matrix factorization: A non-negative factor model with optimal utilization of error estimates of data values, Environmetrics, 5(2), 111–126, doi:10.1002/env.3170050203, 1994.

Petzold, A., Ogren, J. A., Fiebig, M., Laj, P., Li, S.-M., Baltensperger, U., Holzer-Popp, T., Kinne, S., Pappalardo, G., Sugimoto, N., Wehrli, C., Wiedensohler, A. and Zhang, X.-Y.: Recommendations for reporting "black carbon" measurements, Atmos. Chem. Phys., 13(16), 8365–8379, doi:10.5194/acp-13-8365-2013, 2013.

Sandradewi, J., Prévôt, A. S. H., Szidat, S., Perron, N., Alfarra, M. R., Lanz, V. A., Weingartner, E. and Baltensperger, U.: Using Aerosol Light Absorption Measurements for the Quantitative Determination of Wood Burning and Traffic Emission Contributions to Particulate Matter, Environ. Sci. Technol., 42(9), 3316–3323, doi:10.1021/es702253m, 2008.

Ulbrich, I. M., Canagaratna, M. R., Zhang, Q., Worsnop, D. R. and Jimenez, J. L.: Interpretation of organic components from Positive Matrix Factorization of aerosol mass spectrometric data, Atmos. Chem. Phys., 9(9), 2891–2918, doi:10.5194/acp-9-2891-2009, 2009.

Weingartner, E., Saathoff, H., Schnaiter, M., Streit, N., Bitnar, B. and Baltensperger, U.: Absorption of light by soot particles: determination of the absorption coefficient by means of aethalometers, J. Aerosol Sci., 34(10), 1445–1463, doi:10.1016/S0021-8502(03)00359-8, 2003.

Zotter, P., Herich, H., Gysel, M., El-Haddad, I., Zhang, Y., Močnik, G., Hüglin, C., Baltensperger, U., Szidat, S. and Prévôt, A. S. H.: Evaluation of the absorption Ångström exponents for traffic and wood burning in the Aethalometer-based source apportionment using radiocarbon measurements of ambient aerosol, Atmos. Chem. Phys., 17(6), 4229–4249, doi:10.5194/acp-17-4229-2017, 2017.